Journal of Solid State Chemistry **165,** 79–88 (2002)
doi:10.1006/jssc.2001.9496, available online at http://www/idealibrary.com on IDEAL®

Structure, Microstructure, and Mixed Conduction of $[(ZrO_2)_{0.92}(Y_2O_3)_{0.08}]_{0.9}(TiO_2)_{0.1}$

M. T. Colomer[1] and J. R. Jurado

Instituto de Cerámica y Vidrio, CSIC, Antigua Crtra. Valencia Km. 24,300, 28500 Arganda del Rey, Madrid, Spain
E-mail: tcolomer@icv.csic.es

Received August 22, 2001; in revised form November 21, 2001; accepted December 21, 2001

$[(ZrO_2)_{0.92}(Y_2O_3)_{0.08}]_{0.9}(TiO_2)_{0.1}$ (titania-doped yttria stabilized circonia, 10TiYSZ) samples were prepared by solid state reaction from mixtures of 8 mol% yttria-doped ZrO_2 (YSZ) and TiO_2 and characterized in terms of structure, microstructure, and electrical properties. $[(ZrO_2)_{0.97}(Y_2O_3)_{0.03}]_{0.9}(TiO_2)_{0.1}$ (titania-doped tetragonal zirconia polycrystalline, 10TiTZP) was also prepared for comparison in some specific studies. Ionic transport properties were measured by impedance spectroscopy in air as a function of temperature. DC techniques including electromotive force (EMF) and Ion Blocking measurements (IB) were carried out in order to determine the electronic contribution to the total conductivity. The addition of titania to YSZ induces the tetragonal zirconia phase formation, thus $[(ZrO_2)_{0.92}(Y_2O_3)_{0.08}]_{0.9}(TiO_2)_{0.1}$ is a composite material and is constituted by two solid solutions, titania-doped yttria-stabilized zirconia (67.7 mole fraction) and titania-doped tetragonal zirconia (32.3 mole fraction). A decrease in bulk ionic conductivity, of one order of magnitude, when TiO_2 is added to YSZ is observed in the whole temperature range. Furthermore, in the bulk conductivity vs the reciprocal of the temperature plot, a bending (from 550°C to higher temperatures) toward higher activation energies was detected. The bending could indicate the existence mainly of Ti^{4+}–Vö associated pairs with an association energy of 0.43 ± 0.02 eV. It could mean that Ti–O bonds become stronger and shorter and could produce the formation of microdomains of a $ZrTiO_4$-like structure. The addition of titanium is effective in increasing the electronic conductivity under reducing conditions. Conductivity as a function of Po_2 and IB results cannot be related to the formation of small polarons during the reduction process. Furthermore, according to the calculations based on the small polaron theory, inconsistent values for the radius of a small polaron (r_p) are obtained in both 10TiYSZ and 10TiTZP. However, large polarons can explain the transport properties in these materials under reducing conditions in agreement with the experimental data. © 2002 Elsevier Science (USA)

[1]To whom Correspondence should be addressed.

INTRODUCTION

In technological applications such as solid oxide fuel cells (SOFCs), where high current densities are required, the electrode polarization associated with the charge transfer process reduces the cell effectiveness. It is believed that the electrocatalytic effect of the electrolyte surface may improve the efficiency of the cell. The basic idea is that the nature of the electrolyte surface can be modified, at sufficiently high polarization levels, with the formation of intermediate ionized species that will participate in the process as a catalyst (1). To achieve this type of effect, it was also suggested that the electrolyte properties could be changed by doping with appropriate mixed valence cations. Under reducing conditions they change their valence state and enhance both the concentration of oxygen vacancies and the electronic conductivity, which should promote the participation of the electrolyte surface on the anodic process of a SOFC. This "electrocatalytic effect" must be interpreted as an extension of the reaction zone from the triple contact points because of the availability of mobile electronic charge carriers at the surface of the electrolyte in close proximity to oxygen vacancies. Stable mixed ionic and electronic conducting oxides with the fluorite structure show some very attractive characteristics for the use as a matrix in anode materials in SOFCs. Some authors mentioned the use of ceria (2,3), titania (4–10), ruthenium oxide (11, 12), terbia (13), iron (14, 15), and Mn_2O_3 (16) for this purpose. Yttria-stabilized zirconia with 1–12 mol% TiO_2 dopant is considered as a promising candidate for SOFC anodes because they have excellent stability at high temperatures, good compatibility with the YSZ electrolyte, mixed conductivity, and electrocatalytic activity. Furthermore, these mixed oxygen ion–electronic conductors have a potential use as oxygen permeable membranes and electrolyzers.

0022-4596/02 $35.00

It is generally accepted that the ionic conduction in air of titania-doped YSZ decreases with increasing titania content (4–6,8). That fact can be partially explained by the dilution effect because of the substitution of Zr^{4+} by Ti^{4+}, but this only explains a slight overall decrease in concentration of ionic defects. Colomer *et al.* (17), by using XRD and scanning electron microscopy, detected the presence of titania-doped tetragonal zirconia in titania-doped fluorite phase, which could be one of the reasons for the ionic conductivity decrease. Traqueia *et al.* (18) by using Raman spectroscopy also reported tetragonal short-range order in the fluorite phase. However, there has not been a study to separate the possible contributions to decrease the ionic conductivity in the materials of the ternary system ZrO_2–Y_2O_3–TiO_2.

Moreover, the electronic mechanism that takes place under reducing conditions in these materials is still controversial. Naito and Arashi (7) and Lindegaard *et al.* (9) found an increase in conductivity at low oxygen partial pressures, which they ascribed to a small polaron mechanism. According to Marques *et al.* (19) there is no clear evidence of a small polaron mechanism in these materials.

The present work aims at understanding the effect of the addition of titania on the structural, microstructural, and electrical properties of YSZ. Furthermore, the mechanism of the electronic contribution in a reducing atmosphere (small or large polaron) is also studied under experimental and theoretical points of view.

EXPERIMENTAL

This work focuses on $[(ZrO_2)_{0.92}(Y_2O_3)_{0.08}]_{0.9}(TiO_2)_{0.1}$ (10TiYSZ); the rest of the compositions (Table 1) have been considered for some specific studies.

$[(ZrO_2)_{0.92}(Y_2O_3)_{0.08}]_{0.95}(TiO_2)_{0.05}$ (5TiYSZ), $[(ZrO_2)_{0.92}(Y_2O_3)_{0.08}]_{0.9}(TiO_2)_{0.1}$ (10TiYSZ), $[(ZrO_2)_{0.97}(Y_2O_3)_{0.03}]_{0.95}(TiO_2)_{0.05}$ (5TiTZP), and $[(ZrO_2)_{0.97}(Y_2O_3)_{0.03}]_{0.90}(TiO_2)_{0.10}$ (10TiTZP) were prepared by the addition of TiO_2 (Merck, Germany) to YSZ or TZP, respectively (commercially available powders, 8 and 3 mol%, Y_2O_3 respectively, Tosoh, Tokyo, Japan). $[(ZrO_2)_{0.94}(Y_2O_3)_{0.06}]_{0.948}(TiO_2)_{0.052}$ (5.2Ti6Y) and $[(ZrO_2)_{0.98}(Y_2O_3)_{0.02}]_{0.952}(TiO_2)_{0.048}$ (4.8 Ti2Y) were prepared from ZrO_2 (prepared by hydrolysis from $Zr(OCH_2CH_2CH_3)_4$ (Aldrich, USA), Y_2O_3 (Johnson Matthey GmbH, England), and TiO_2 (Merck, Germany) mixtures.

YSZ, TZP, and the powder mixtures were submitted to attrition milling for 2 h, sieved (63 μm) and calcined at 800°C for 2 h and sieved again (63 μm). Finally, the powder was pressed isostatically at 200 MPa into bars that were cut to prepare discs for electrical measurements. YSZ, 5TiYSZ, and 10TiYSZ samples were sintered in air at 1500°C for 2 h (heating and cooling rate 5°C/min). TZP, 5TiTZP, and 10TiTZP samples were sintered at 1400°C for 2 h in air (heating and cooling rate 5°C/min). Final densities were measured by the Archimedes' immersion method in water. X-ray diffraction patterns of the samples were obtained using a Siemens D-5000 diffractometer and monochromated high-intensity Cu$K\alpha_1$ radiation ($\lambda = 1.5405$ Å). The experimental diffraction patterns were collected at room temperature over a range of $20 \leq 2\Theta \leq 80$ (step-scanned at 1°/5 s). For lattice parameter determination, the studied range was $33 \leq 2\Theta \leq 80$ (step-scanned at 0.025°/20 s). The experimental diffraction patterns for the phase distribution calculations were collected at room temperature over a range of $71 \leq 2\Theta \leq 75$ (step-scanned at 0.025°/20 s).

TABLE 1
Compositions Considered in This Work

Material	Label
$(ZrO_2)_{0.92}(Y_2O_3)_{0.08}$	YSZ
$[(ZrO_2)_{0.92}(Y_2O_3)_{0.08}]_{0.95}(TiO_2)_{0.05}$	5TiYSZ
$[(ZrO_2)_{0.92}(Y_2O_3)_{0.08}]_{0.90}(TiO_2)_{0.10}$	10TiYSZ
$[(ZrO_2)_{0.94}(Y_2O_3)_{0.063}]_{0.948}(TiO_2)_{0.052}$	5.2Ti6Y
$[(ZrO_2)_{0.98}(Y_2O_3)_{0.021}]_{0.952}(TiO_2)_{0.048}$	4.8Ti2Y
$(ZrO_2)_{0.97}(Y_2O_3)_{0.03}$	TZP
$[(ZrO_2)_{0.97}(Y_2O_3)_{0.03}]_{0.95}(TiO_2)_{0.05}$	5TiTZP
$[(ZrO_2)_{0.97}(Y_2O_3)_{0.03}]_{0.9}(TiO_2)_{0.1}$	10TiTZP

The phases distribution (mole fractions) (20) in the sintered materials were determined by the ratio

$$\frac{M_c}{M_t} = 0.88\frac{I_c(400)}{I_t(400) + I_t(004)} \quad [1]$$

The microstructure of the sintered samples was analyzed on polished and thermally etched surfaces by means of scanning electron microscopy energy-dispersive X-ray (SEM-EDX) (Model DSM 950, Zeiss, Oberchen, Germany). The grain size was determined using automatic image analysis (Model IMAGIST V6, Princeton Gamma Tech. Inc., Princeton, NJ) of SEM micrographs, and the mean grain size was obtained by considering the equivalent spherical diameter of at least 200 grains.

Samples prepared as pellets with 0.8 cm diameter and thickness 0.2 cm were electroded with platinum high-conductivity paste on both sample surfaces. Electrochemical impedance spectroscopy (EIS) analysis in air and under reducing atmosphere, between 250 and 1000°C, by using computer-assisted electromotive force (EMF) readings during the reduction and/or oxidation of the furnace atmosphere was performed. The impedance analyzer used was a HP 4192A in the frequency range of 10 to 10^7 Hz.

10TiYSZ and 10TiTZP were treated under reducing conditions (10^{-18} atm.) for 2 h in order to evaluate the possible weight losses due to a partial reduction.

Impedance spectroscopy measurements at constant frequency (10 KHz) in a controlled-atmosphere furnace (21) as a function of temperature (800–1000°C) were performed. The atmosphere was fitted with a YSZ oxygen sensor to ensure continuous monitoring of the oxygen partial pressure next to the pellet being characterized. The furnace atmosphere can be brought quickly from air to reducing conditions by a single flushing of the closed furnace chamber with a $N_2 + H_2$ gas mixture. Data can be obtained while reducing or raising the Po_2 of the furnace atmosphere. The latter is usually preferred, and it corresponds to a slow transition in Po_2 due to the permeation of oxygen through the sensor tube (electrochemical) and other possible minor physical leaks in the system. A complete redox cycle usually takes more than 8 h.

Measurement of the ionic transport number was performed in the above-mentioned furnace, including a YSZ sensor and a YSZ electrochemical pump, for oxygen pressure control. The open circuit (EMF) measurements were performed with a concentration cell using air as a reference: Po_2 (variable), Pt || Sample ||Pt, air (reference).

The experimental data consist of the cell EMF against the EMF of a reference YSZ sensor, and are continually recorded by a data acquisition system during the reduction or reoxidation of the furnace atmosphere. The furnace atmosphere is brought from oxidizing to reducing conditions by the electrochemical pumping of oxygen. An automatic data acquisition system enables continuous recording of the sensor and sample open circuit.

The ion blocking technique (19) employed an impervious alumina disk sealed with a Pyrex ring against one side of the mixed conductor pellet (blocking electrode). A reversible Pt electrode on the other side of the pellet in contact with air was used as the reference electrode. A dc source was used to establish a constant applied voltage to the cell. High-impedance multimeters and a resistor in series with the cell were used to perform the voltage and current measurements, as shown in Fig. 1.

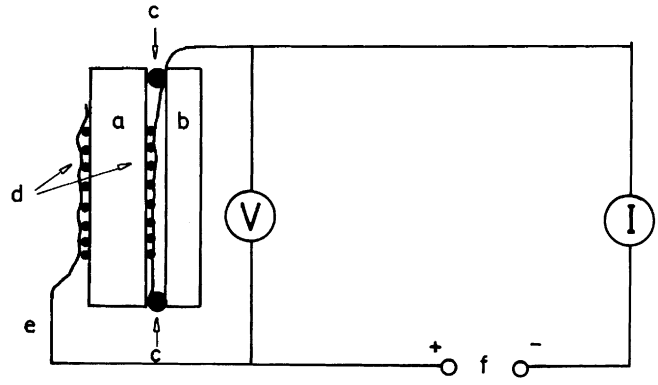

FIG. 1. Experimental setup used in ion-blocking measurements: (a) mixed conductor, (b) alumina disk, (c) Pyrex seal, (d) Pt electrodes, (e) Pt wires, (f) dc source, and (g) resistor.

RESULTS AND DISCUSSION

X-Ray Diffraction Analysis

For the 10TiYSZ material, peaks corresponding to cubic and tetragonal zirconia are observed. All *d* spacing values (cubic and tetragonal symmetries) are shifted with respect to YSZ and TZP, indicating the existence of two titania solid solutions. The percentage of cubic zirconia was calculated to be 67.7 mole fraction and the tetragonal phase was 32.3 mole fraction. It is clear that the dopant destabilizes the cubic phase and induces the formation of tetragonal zirconia. It is well known that tetravalent dopants smaller than zirconium ions do not form cubic zirconia solid solutions (22). However, when 5 mol% of titania is added to YSZ, only a solid solution of cubic zirconia is detected.

The lattice parameters were 0.5137 ± 0.0005 and 0.5122 ± 0.0005 nm for YSZ and 10TiYSZ, respectively. This lattice decrease can be due to the replacement of the Zr^{4+} ions by the smaller Ti^{4+} ions. Obviously, the lattice volume is smaller for 10TiYSZ than for YSZ (see Table 2).

10TiTZP shows only peaks of tetragonal symmetry. The cell volume also decreased with the titania addition to TZP. This can also be interpreted as a lattice distortion for the replacement of the Zr^{4+} ions by Ti^{4+}. Table 2 summarizes the lattice volume values for the compositions studied.

As mentioned above, the addition of TiO_2 to YSZ induces the formation of tetragonal zirconia. In the cubic zirconia the coordination of Zr^{4+} is 8 (equal distances), whereas in the tetragonal lattice the distances are not the same (6 + 2) (18). Thus, the latter case is closer than that of the rutile-type structure, where the Ti^{4+} is six-coordinated. This fact could be the reason why the addition of titanium leads to the formation of tetragonal zirconia. As a consequence, the solubility limit of titania in YSZ is quite small (slightly higher than 5 mol%), according to the isothermal section outlined by Colomer *et al.* (17), when compared to other dopants with similar structures (3).

Relative Densities

Table 3 shows the relative densities of the samples after sintering. As can be seen, the addition of titania is effective in inducing full density compact bodies in both tetragonal and fluorite phases, in agreement with the well-known effect of titania as sintering aid (23).

Scanning Electron Microscopy Energy-Dispersive X-Ray Microanalysis (SEM-EDX)

A typical microstructure of 10TiYSZ sintered in air at 1500°C for 2 h, after polishing and thermal etching, is shown in Fig. 2. Fully densified bodies were obtained for 10TiYSZ in comparison with undoped YSZ, which

TABLE 2
Cubic and Tetragonal Phase Contents (mole Fraction) and Lattice Volumes for Sintered Samples

Material	% Cubic phase	% Tetragonal phase	Lattice volume cubic phase (nm^3)	Lattice volume tetragonal phase (nm^3)
YSZ	100.0	0.0	0.1356 ± 0.0002	—
5TiYSZ	100.0	0.0	0.1348 ± 0.0002	—
10TiYSZ	67.7	32.3	0.1344 ± 0.0002	0.1330 ± 0.0002
TZP	0.0	100.0	—	0.1340 ± 0.0002
5TiTZP	0.0	100.0	—	0.1336 ± 0.0002
10TiTZP	0.0	100.0	—	0.1330 ± 0.0002

exhibited inter- and intragranular porosity. A bimodal grain size distribution is observed for 10TiYSZ. Large grains with an average grain size of 4.0 μm and small grains with an average size of 1.0 μm were noted. By EDX semiquantitative analysis it is seen that the large grains have approximately 6.0 mol% of Y_2O_3, whereas the small grains have 2.0 mol% of Y_2O_3. The EDX analysis also indicates that the TiO_2 concentration is 5.2 and 4.8 mol% for cubic and tetragonal grains, respectively. It agrees well with the solid solution limit of titania into YSZ (slightly higher than 5 mol%) obtained from the isothermal section in this system at 1500°C (17). Conclusively, the 10TiYSZ material consists of two phases, namely $[(ZrO_2)_{0.94}(Y_2O_3)_{0.063}]_{0.948}(TiO_2)_{0.052}$ (5.2Ti6YSZ) and $[(ZrO_2)_{0.98}(Y_2O_3)_{0.021}]_{0.952}(TiO_2)_{0.048}$ (4.8Ti2Y). Furthermore, the EDX analysis indicated uniform concentrations of the solid solution components along the grain boundaries and in the center of large and small grains.

Figure 3 shows $ZrTiO_4$ precipitates on the cubic grains after severe thermal etching (1480°C for 15 min). The EDX analysis showed an increase in intensity of the Ti peaks for the precipitates compared to those for the cubic and tetragonal zirconia phases. The XRD pattern of this thermally etched sample indicated the presence of a $ZrTiO_4$ phase attributable to the precipitates. The segregation takes place on cubic grains that have a higher amount of titania. Furthermore, the solid solubility limit is higher for titania-doped TZP (higher than 10 mol% titania) than for titania-doped YSZ (lower than 10 mol% Titania).

TABLE 3
Relative Densities of YSZ, 5TiYSZ, 10TiYSZ, 5TiTZP, and 10TiTZP

Sample	Relative density (%)	Sintering temperature and time
YSZ	93.0 ± 0.5	1500°C/2 h
5TiYSZ	96.7 ± 0.5	1500°C/2 h
10TiYSZ	99.9 ± 0.5	1500°C/2 h
TZP	94.0 ± 0.5	1400°C/2h
5TiTZP	98.0 ± 0.5	1400°C/2 h
10TiTZP	99.9 ± 0.5	1400°C/2 h

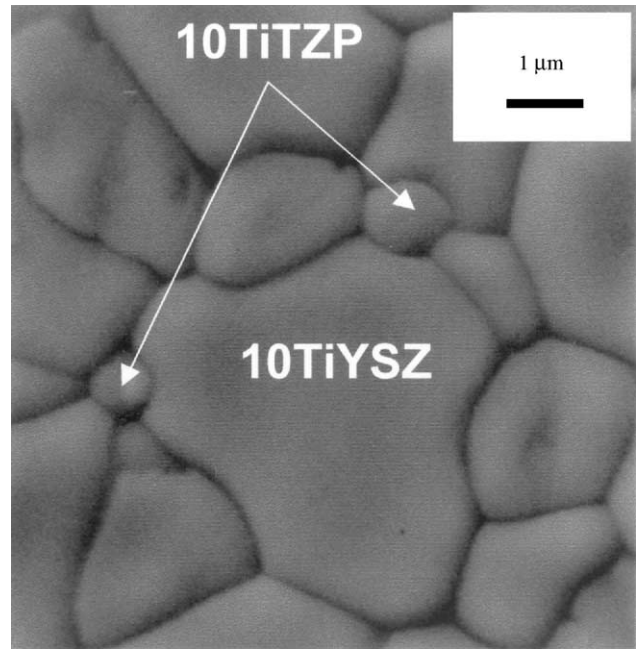

FIG. 2. SEM micrograph of 10 TiYSZ sintered at 1500°C for 2 h.

AC Electrical Measurements

Impedance spectroscopy measurements in air. Impedance spectroscopy measurements were performed at temperatures ranging from 300 to 1000°C. From the impedance plots (Fig. 4) obtained, the bulk and the grain

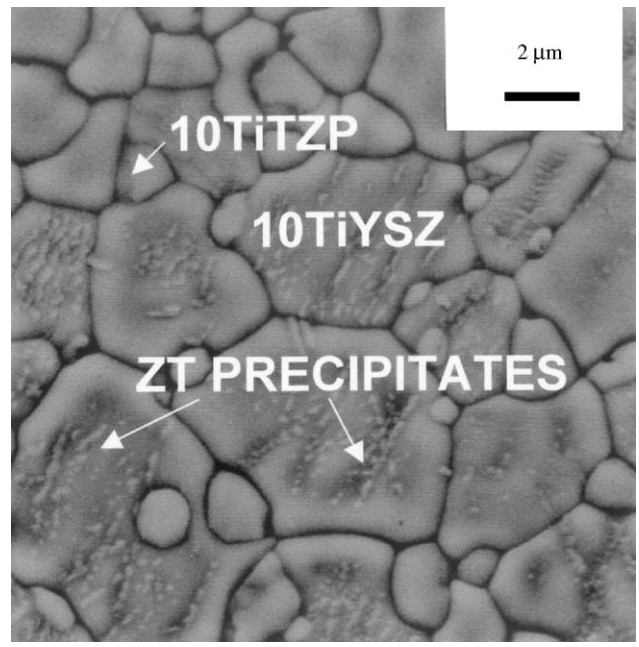

FIG. 3. SEM micrograph of 10TiYSZ with precipitates of $ZrTiO_4$ (ZT).

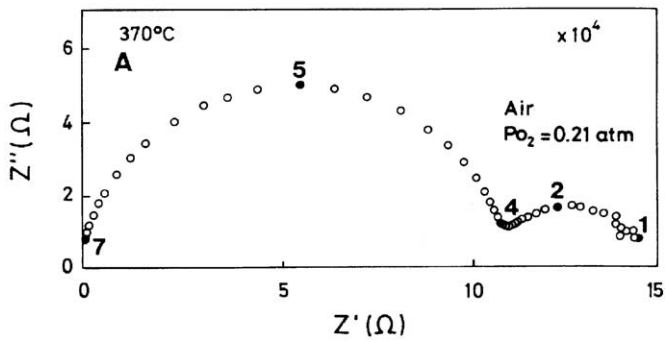

FIG. 4. Impedance spectrum for 10TiYSZ at 370°C in air.

boundary contributions can be easily separated. The bulk resistance was considered to be the intersection of the arc at high frequencies with the real axis. The grain boundary resistance corresponds to the intersection of the arc at low frequencies with the real axis. The total resistance was considered to be the sum of the grain boundary and the lattice resistances.

Data for 10TiYSZ indicate that the addition of titania results mostly in increasing bulk resistance of the material, corresponding to an overall conductivity drop of about one order of magnitude (nine times) when compared to YSZ (Fig. 5). Dilution effect, because of the substitution of Zr^{4+} by Ti^{4+}, has a negligible effect on the bulk resistivity reduction of both phases (tetragonal and fluorite phases).

The effect of dopants on conductivity usually takes into consideration the effective pathway for oxygen ions moving between adjacent sites, which promotes the free radius effect. Based on the ionic radius of Zr^{4+} (VIII) = 0.084 nm and Ti^{4+} (VIII) = 0.074 nm (24), it can be concluded that the substitution of Zr^{4+} by Ti^{4+} causes an increment in the free radius. This is expected to yield an increase in ionic conductivity and a decrease in the activation energy for ionic mobility. However, the results are contradictory to experimental evidence. In this work, the simple effect of the dopant cation radius is believed not to be a significant parameter in the resistivity enhancement.

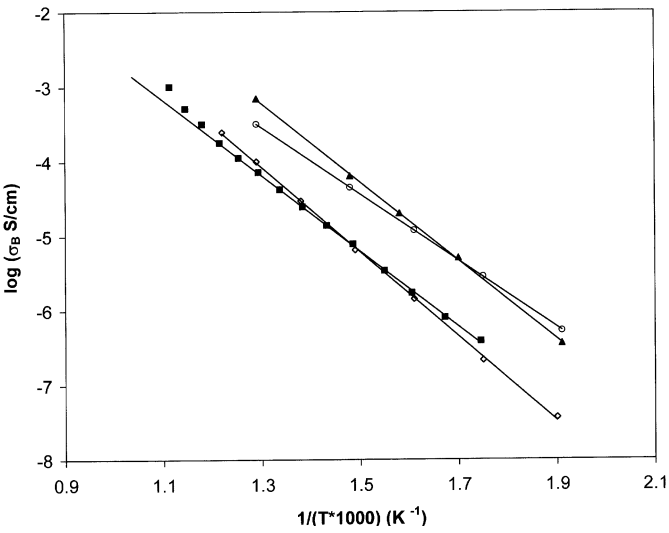

FIG. 5. Log of the bulk σ in air for YSZ (▲), 10TiYSZ (■), TZP (○) and 10TiTZP (◇) versus the reciprocal of the temperature.

The above-mentioned effects cannot explain the bulk conductivity drop in 10TiYSZ of one order of magnitude with respect to YSZ. The next sections try to explain why there is a large difference between the bulk conductivity for 10TiYSZ and that for YSZ.

Calculation of the increment of resistivity in air due to the presence of both cubic and tetragonal phase solid solutions. As a first approach the bulk resistivity value for 10TiYSZ can be calculated by the empirical mixture rule:

$$\rho_{\text{bulk}}(\text{10TiYSZ}) = \rho_{\text{bulk}}(\text{cubicphase}) \times f(\text{cubicphase}) + \rho_{\text{bulk}}(\text{tetragonalphase}) \times f(\text{tetragonalphase}) \quad [2]$$

$$\rho_{\text{bulk}}(\text{10TiYSZ}) = \rho_{\text{bulk}}(\text{5.2Ti6Y}) \times f(\text{5.2T6Y}) + \rho_{\text{bulk}}(\text{4.8Ti2Y}) \times f(\text{4.8Ti2Y}), \quad [3]$$

where f (5.2Ti6Y) and f (4.8Ti2Y) are the volume fractions of the cubic and tetragonal phases, respectively. These values are obtained from XRD data: 0.68 volume fraction (cubic phase) and 0.32 volume fraction (tetragonal phase), respectively, as mentioned under X-Ray Diffraction Analysis.

The fluorite phase (5.2Ti6Y) has a bulk resistivity at 500°C of $2.24 \times 10^3\,\Omega \times \text{cm}$, whereas the tetragonal composition (4.8Ti2Y) has a bulk resistivity of $6.3 \times 10^3\,\Omega \times \text{cm}$ at the same temperature. The experimental value for the ρ_{bulk} of 10TiYSZ is $1.41 \times 10^4\,\Omega \times \text{cm}$ and if Eq. [3] is applied, a value of $3.56 \times 10^3\,\Omega \times \text{cm}$ is obtained. The difference between these values is 1.05×10^4, which is 75% of the bulk resistivity. This discrepancy between these values is believed due to the existence of structural modifications and their effects on the bulk resistivity in both cubic and tetragonal lattices, in 10TiYSZ (see Table 2). According to Colomer *et al.* (17) and Feighery *et al.* (25) with increasing Y^{3+} content, the stabilized cubic fluorite phase can incorporate much more Ti^{4+}. This is probably because the highly defective fluorite structure contains a large number of oxygen vacancies. This enables Ti^{4+} to assume its preferred sixfold coordination. When Y^{3+} content is low (10TiTZP), the number of oxygen vacancies is low and Ti^{4+} ions trap oxygen vacancies to move away from eightfold coordination of the Zr^{4+} site. It provokes a

TABLE 4
Activation Energies and Bulk Resistivity Increment Due to Structural Changes for Different Materials

Material	Ea (eV) bulk	Ea (eV) total	$\Delta \rho_{SM}$ (%) at 500°C
YSZ	1.00±0.02	1.04±0.01	—
5TiYSZ	0.98±0.03	—	50
10TiYSZ	0.96±0.03	1.00±0.03	75
TZP	0.85±0.01	0.87±0.01	—
5TiTZP	1.04±0.02	—	61
10TiTZP	1.07±0.02	0.92±0.01	68

strong change in its structure. This vacancy trapping effect is related to the high bulk activation energy value (1.07±0.02 eV) for TiTZP compared to that for TZP (0.85±0.02 eV) (see Table 4). By using Raman spectroscopy Traqueia *et al.* (18) confirmed the latter assumptions that showed that the anion sublattice is composed of tetragonal- and cubic-like domains having different conductivities mainly because of the lower oxygen vacancy content in the tetragonal-like domains. They proposed that this decrease in the vacancy concentration is due to the Ti ions, which trap oxygen vacancies to shift from the eightfold-coordinated Zr site toward their preferred sixfold coordination. A simple explanation would be that oxygen migration occurs mostly in the disordered regions. As the titania content increases, these regions disappear and the electrical conductivity decreases.

5TiYSZ, which does not have any tetragonal phase, exhibits a bulk resistivity increase of 50% with respect to undoped YSZ. Again, neither the dilution effect nor the free radius effect has a significant effect on that bulk resistivity increment. Structural modifications could therefore be responsible for that increment.

Conclusively, one order of magnitude increment of the resistivity for 10TiYSZ in comparison to that for YSZ could be explained by considering the ρ value given by Eq. [2], but this increment may be caused by the strong structural modifications suffered when Ti^{4+} ions are introduced into the cubic and tetragonal lattices.

Arrhenius Plots. Activation energy. If the temperature range between 200 and 500°C is considered for both YSZ and 10TiYSZ, the values of the bulk activation energy, 1.00±0.02 and 0.96±0.03 eV, respectively, are independent of the titania content (Fig. 5). This fact coincides with the findings in other works (18,26,27). It means that a further addition of titania does not modify the conduction mechanism in the temperature range mentioned. The curve that corresponds to 10TiTZP overlaps in a narrow range of temperature with that of 10TiYSZ. However, the activation energy is slightly higher for 10TiTZP (1.07±0.02 eV) than for 10TiYSZ (0.96±0.03 eV) (see Table 4). This fact can be explained by a structural modification taking place in TZP stronger than that taking place in YSZ, as mentioned above.

A bending toward a higher activation energy was found in the σ_B versus $1/T$ Arrhenius plot for 10TiYSZ from 550°C to higher temperatures (Fig. 5). The bending has an activation energy of 1.39±0.03 eV, which means an association energy of 0.43±0.02 eV. This large value can only be explained by the formation of strong associated pairs, Ti^{4+}–$V_{ö}$. The same bending effect is also reported by Naito and Arashi for $(ZrO_2)_{0.8}(TiO_2)_{0.1}(Y_2O_3)_{0.1}$ (7), who suggested that this activation energy change is the intrinsic behavior of the TiO_2-doped YSZ. This intrinsic feature could be related to an enhancement of Ti^{4+}–$V_{ö}$ interactions when the temperature is raised. Presumably, the concentration of Ti^{4+}–$V_{ö}$ pairs is augmented as temperature increases.

Li *et al.* (22) by using X-ray absorption spectroscopy in GeO_2-doped tetragonal zirconia observed that the Ge–O bond is shorter and stronger than that of the Zr–O bond. Note that Ge and Ti cations both are tetravalent dopants and their ionic radius is smaller than that of Zr^{4+}. These authors suggest a local Ge–Zr ordering and the formation of a scheelite-like Zr_3GeO_4 structure. In this work, the increase in activation energy suggests that the Ti–O distances could be shorter and could produce the formation of microdomains that contain the trapped vacancies. A local ordering can be suggested in 10TiYSZ, since a thermal etching very close to the sintering temperature reveals the presence of $ZrTiO_4$, as mentioned above (Fig. 3).

Figure 6 shows the Arrhenius plot of the total conductivity as a function of the reciprocal of the temperature for 10TiYSZ. The total conductivity for 10TiYSZ does not exhibit the usual high-temperature bending (toward lower activation energy values) found for YSZ. The absence of that bending could be ascribed to the

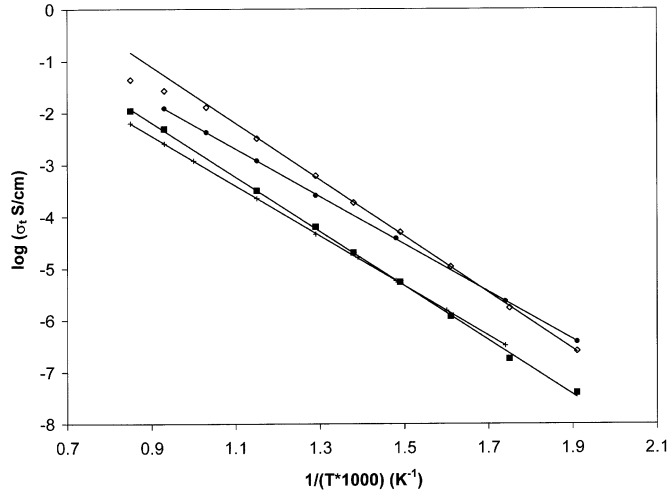

FIG. 6. Log of the total σ in air for YSZ (◇), 10TiYSZ (■), TZP (●), and 10TiTZP (+) versus the reciprocal of the temperature.

presence of the tetragonal zirconia phase. TZP and titania-doped TZP materials do not exhibit any bending in their curves (Fig. 6). This fact can be related to an association energy in tetragonal zirconia higher than that in cubic zirconia.

Dependence of electrical conductivity on Po_2. Figure 7 shows the dependence of electrical conductivity at 10 KHz and 1000°C on oxygen partial pressure for 10TiYSZ and 10TiTZP. That frequency was chosen because the impedance spectra showed that 10 KHz is located where the material response takes place. All curves obtained at different temperatures (800–1100°C) and at 10 KHz exhibit identical dependencies on the oxygen partial pressure for 10TiYSZ. Following a plateau at moderately oxidizing conditions, the conductivity increases with increasingly reducing conditions. The onset of electronic conductivity under reducing conditions can exhibit either a $-\frac{1}{4}$ or a $-\frac{1}{6}$ Po_2 dependence. (7,9). The first result is to be expected when the increase in electronic defects is associated with the reduction of titanium ions in the cation sublattice:

$$O_o + 2Ti_{zr} = V_{\ddot{o}} + 2Ti'_{zr} + \tfrac{1}{2}O_2\,. \qquad [4]$$

In this reaction the Kröger–Vink type of notation has been assumed for defects. The symbol Ti_{Zr}' corresponds to an electronic defect localized in a titanium ion in the cation sublattice (small polaron). The behavior expected for such localized electronic defects could be confirmed by electronic ion-blocking measurements

On assuming a reduction process occurring in a titanium-rich grain boundary, the concentration of electronic defects might be compensated by the formation of oxygen vacancies:

$$|Ti_M|_{g.b.} \propto Po_2^{-1/6}. \qquad [5]$$

The $-\frac{1}{6}$ Po_2 dependence corresponds to neglecting the role of yttrium ions in determining the concentration of negative defects in the grain boundary.

Reasonable estimates for the ionic conductivity were obtained in both cases. However, the results obtained correspond to poor correlation factors in both cases. An additional difficulty in assessing a clear Po_2 dependence results from the unknown effect on oxygen vacancies under reducing conditions. Those findings were also reported in titania-doped cubic zirconia sintered at 1300 or 1600°C for 2 h (28).

The model used for data analysis is clearly inconclusive. Ion-blocking measurements could clarify the electronic transport properties.

For 10TiTZP all curves obtained from 800 to 1100°C exhibit identical dependencies on Po_2, and it is also observed that the dependence does not follow either a $-\frac{1}{4}$ or a $-\frac{1}{6}$ slope (Fig. 7). Again, the fitted results obtained for the 10TiTZP material are poorly correlated.

The presence of the tetragonal phase in 10TiYSZ seems not to affect the conductivity mechanism under reducing conditions. In neither the 10TiYSZ nor the 10TiTZP sample was the typical maximum of a small polaron mechanism in the log versus Po_2 detected.

The transport properties of 10TiYSZ are not only evaluated from ac conductivity measurements as a function of oxygen partial pressure because these measurements are insensitive to minor electronic contributions. Additional techniques to separate the ionic and electronic conductivity contributions are required. This is achieved by dc techniques, such as open circuit EMF and the ion-blocking electrode technique (19).

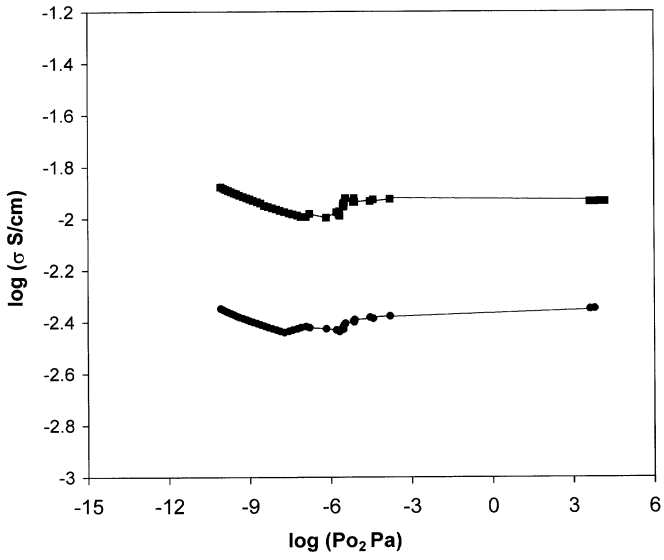

FIG. 7. Dependence of electrical conductivity (10 KHz) on oxygen partial pressure for both 10 TiYSZ (■) and 10 TiTZP (●) at 1000°C.

DC Electrical Measurements

Ionic transport number. Electromotive force (EMF) measurements. Figure 8 shows data of EMF values for 10TiYSZ at 1000°C within a small range of reducing oxygen partial pressures. The ionic transport number of this composition was found to be typically one in air, and decreases with decreasing Po_2, as shown in Fig. 8. This decrease indicates the onset of electronic conductivity under reducing conditions and is related to the reduction of titanium ions.

An accurate data treatment should be used to characterize mixed conductor materials when considering their utilization in a narrow range of oxygen partial pressures. In this case, the most useful parameter is the effective ionic transport number, defined as

$$t_i = \left(\frac{4F}{RT}\right)\frac{d(\mathrm{EMF})}{d(\ln Po_2)} \qquad [6]$$

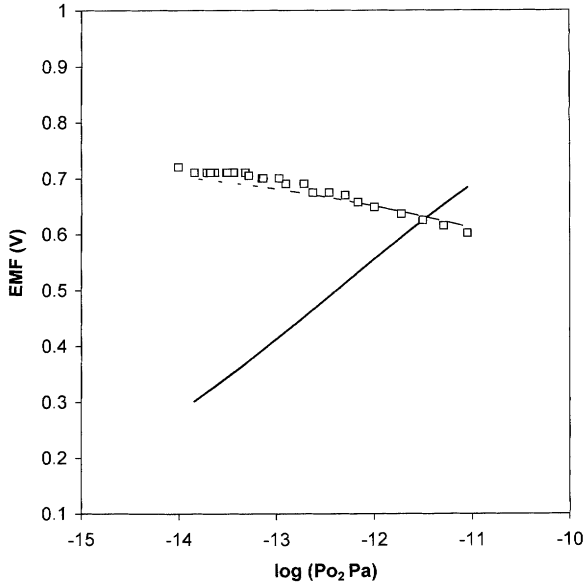

FIG. 8. Open circuit EMF data (□) obtained with an oxygen concentration cell based on a 10TiYSZ disc at 1000°C. The EMF dashed line and the t_i solid line correspond to estimates based on curve fitting.

In the oxygen pressure range, where the concentration of ionic defects is determined by the concentration of dopant (yttrium oxide) and the concentrations of holes and electrons are proportional to the $+\frac{1}{4}$ and $-\frac{1}{4}$ power of the oxygen partial pressure, respectively, the ionic transference number can be expressed as

$$t_i = \frac{1}{(1 + A\mathrm{Po}_2^{-1/4} + B\mathrm{Po}_2^{1/4})}. \qquad [7]$$

In this expression, A is the electronic to ionic conductivity ratio for unit oxygen partial pressure. The B coefficient is the analogous ratio for electron hole conductivity. Incorporating Eq. [7] into Eq. [6] and integrating this equation over the appropriate limits of oxygen partial pressure, an expression where the cell EMF is a function of A, B, and the oxygen partial pressure boundary conditions can be obtained (19). The experimental data can be fitted to this equation and the parameters A and B estimated (as found in the present situation). The p-type conductivity contribution for 10TiYSZ is insignificant for oxygen partial pressures lower than ambient air ($\mathrm{Po}_2 = 0.21$ atm). For this reason, the value of B can be neglected in the Eq. [7]. The A coefficient is the most relevant parameter to determine the ionic transport number under reducing conditions, (Eq. [7]). Based on this estimate, the dependence of EMF and t_i on Po_2 was also plotted in Fig. 8, and it can be seen that the ionic transport number of this composition is quite small under reducing conditions.

The EMF dependence on the oxygen partial pressure can be obtained by the equation

$$V = \frac{RT}{4F} \int t_i d \ln \mathrm{Po}_2. \qquad [8]$$

The evaluation of the relevance of the electronic conductivity component can be made by simple evaluation of the ratio of EMF sample/EMF sensor, which gives us an average ionic transport number between air and the oxygen pressure limiting conditions corresponding to the sensor EMF values used in the calculation. According to this type of calculation, the average ionic transport number between air and 9.83×10^{-15} Pa at 1000°C is 0.78, which indicates a significant electronic conductivity component. For 10TiTZP similar results were achieved. Samples treated under reducing conditions suffered low weight losses (2%), in agreement with that obtained by Marques *et al.* (29). It suggests that the level of Ti^{4+} reduction achieved is also low. This result, together with the observation of the high electronic conductivity contribution, indicates that the mobility of the electronic defects may be much higher than usually reported for a small polaron. This result is in agreement with Marques *et al.* (19).

Ion-Blocking Measurements

Ion-blocking measurements were performed on the 10TiYSZ samples. Results obtained with this technique at temperatures between 700 and 1000°C are shown in Fig. 9.

The enhancement in electronic conductivity is determined by the formation of mobile electronic defects in the titania-doped YSZ materials related to the reduction of titanium ions as mentioned above. At low temperature (700°C), the behavior of 10TiYSZ tends to be similar to YSZ, indicating minor enhancement in electronic conductivity for as expected a small concentration of Ti^{3+}.

The expected behavior of 10TiYSZ can be derived starting from the dc equivalent circuit suggested by

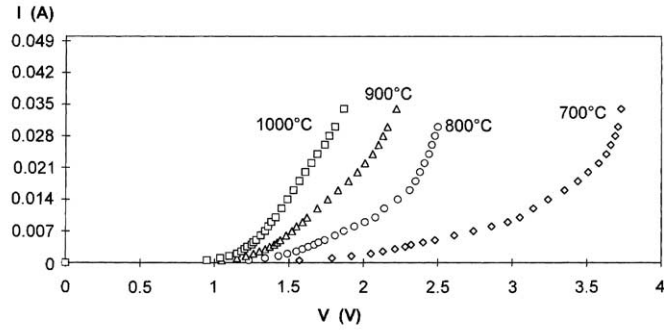

FIG. 9. *I–V* plots for 10TiYSZ from 700 to 1000°C obtained by ion-blocking technique.

Patterson *et al.* (30) to describe the electrical transport in mixed conductors. The relation between electronic current (I_e) and applied voltage (V) is

$$I_e = \left(\frac{SRT}{FL}\right) \bullet \left\{ \sigma_n^*(e^u - 1) + \sigma_p^*(1 - e^{-u}) + K_\alpha \left[\left(K_\beta + P_{\text{ref}}^{1/4} e^{-u}\right)^{-1} - \left(K_\beta + P_{\text{ref}}^{1/4}\right)^{-1} \right] \right\}, \quad [9]$$

where $u = VF/RT$, S and L are the cell electrode area and thickness, σ_n^* and σ_p^* the electron and hole conductivities at a fixed oxygen partial pressure (at the reversible electrode, P_{ref}), and R, T, and F have their usual meaning. When plotting I_e versus V, based on Eq. [9], a plateau related to the small polaron hopping electronic conductivity contribution should be observed. The intermediate plateau predicted by Eq. [9] is not observed for titania-doped YSZ at any studied temperature.

Experimental evidence obtained for 10TiYSZ is not coherent with the behavior predicted for a mixed conductor with a small polaron conductivity contribution. In fact this plateau can only be expected when the mixed valence dopant is sufficiently reduced, and on assuming a small polaron electronic conductivity contribution.

Note that an applied voltage of 2 V at 1000°C corresponds to an interfacial oxygen partial pressure on the order of 10^{-15} Pa and the corresponding level of reduction of Ti^{4+} ions should be significant. The formation of delocalized electronic defects rather than localized defects may be an alternative explanation for the electronic contribution in this material. Therefore, large polarons instead of small polarons are the most probable mechanism.

Polaron mechanism under reducing conditions . Regarding both the nonexistence of any maximum in the conductivity vs Po_2 plots at low Po_2 values and any plateau in the I–V curves for the ion-blocking measurements, calculations based on the small polaron theory (SPT) (31) were performed in order to confirm the experimental findings.

Polaronic conduction is a typical electron–phonon coupling process; the magnitude of the coupling factor can produce a large or a small polaron radius, r_p. When the polaron effective mass (m_p) is high (10–100 times m^* (electron effective mass)) and its kinetic energy is negligible, r_p is lower than the interionic distance and a small polaron is present. The activation hopping energy of the small polaron is

$$W_H = [-e^2/4\Pi\varepsilon_0 R)](1/\varepsilon_\infty - 1/\varepsilon_s), \quad [10]$$

where e is the electron charge, ε_0 the vacuum dielectric constant, ε_∞ the high-frequency permittivity, ε_s the low-frequency dielectric constant, and R the interionic distance ($Ti^{3+} \Leftrightarrow Ti^{4+}$) between equivalent sites for hopping. It means that the small polaron hopping is effective if Ti^{3+} and Ti^{4+} ions have the same oxygen coordination number.

The basic criterion for the large polaron theory (LPT) is the smallness of the ratio, R/r_p. In this case the motion of the polaron can be described by the Boltzmann equation. Here the polaron is considered as a particle, with an effective electronic mass, m_p, undergoing collisions with phonons (lower excitation levels), which are close to those of the ordinary band theory.

Several authors (4, 7) have proposed a small polaron transport in TiO_2–YSZ materials under reducing conditions. However, titania-doped YSZ mixed conductors are being evaluated mostly from high-temperature conductivity measurements as a function of oxygen partial pressure.

Assuming that our 10TiYSZ under reducing conditions fits the small polaron mechanism and applying Eq. [8] where the value of ε_∞ is 24.24 for 10TiYSZ, that of ε_s is 250, and that of ε_0 is 8.85×10^{-12} F/m, then $1/\varepsilon_s$ is negligible. In order to determine, the small polaron radius, r_p, it is necessary to calculate the interionic distance, R, by means of Eq. [8]. We can use the data of the total conductivity versus oxygen partial pressure. The conductivity values of a specific oxygen partial pressure (10^{-15} Pa), at various temperatures, were taken and plotted as a function of the reciprocal of the temperature. The slope of the straight line gives a hopping activation energy of 1.15 ± 0.05 eV. Assuming that the latter value corresponds to the small polaron hopping activation energy W_H and introducing that value into Eq. [10], the estimated interionic distance (R) between Ti^{3+} and Ti^{4+} ions for 10TiYSZ was 0.52 Å, which is inconsistent with SPT. Inconsistent results with SPT are also achieved for 10TiTZP.

Conclusively, for both materials large polarons, instead of small polarons, could be a possible electronic transport mechanism under reducing conditions.

CONCLUSIONS

10TiYSZ is composed of two phases with approximated compositions of 5.2Ti6Y (titania-doped cubic zirconia) and 4.8Ti2Y (titania-doped tetragonal zirconia) for each phase. Therefore, 10TiYSZ is a ceramic composite. In the bulk conductivity vs the reciprocal of the temperature plot a bending (from 550°C to higher temperature) toward higher activation energy was detected. The bending could indicate the existence of Ti^{4+}–$V_{\ddot{o}}$ associated pairs with an association energy of 0.43 ± 0.02 eV. It could mean that Ti–O bonds become stronger and shorter and could produce the formation of microdomains of $ZrTiO_4$-like structure. The structural modifications in both the cubic and tetragonal

phases by the addition of titania produces an increment in the bulk resistivity of 75%.

In both 10TiYSZ and 10TiTZP, the dependence of the conductivity on Po_2 does not follow either a $-\frac{1}{4}$ or $-\frac{1}{6}$ slope and a maximum in the conductivity versus Po_2 plot is not observed. For 10TiYSZ, the average ionic transport number between air and 9.83×10^{-15} Pa at 1000°C is 0.78 according to the electromotive force measurements, which indicates a significant electronic conductivity component.

Experimental evidence obtained from ion blocking measurements for 10TiYSZ is not coherent with the behavior predicted for a mixed conductor with a small polaron conductivity contribution. Furthermore, according to the calculations based on the small polaron theory, inconsistent values for the radius of a small polaron (r_p) are obtained in both 10TiYSZ and 10TiTZP. However, large polarons can explain the transport properties in these materials under reducing conditions in agreement with the experimental data.

REFERENCES

1. E. J. L. Schouler, *Solid State Ionics* **9–10,** 945 (1982).
2. B. Calès and J. F. Baumard, *J. Electrochem. Soc.* **131,** 2407 (1983).
3. P. V. Ananthapadmanabhan, N. Venkatramani, V. K. Rohatgi, A. C. Momin, and K. S. Venkateswarlu, *J. Eur. Ceram. Soc.* **6,** 111 (1990).
4. S. S. Liou and W. L. Worrell, *Appl. Phys. A* **49,** 25 (1989).
5. R. M. C. Marques, J. R. Frade, and F. M. B. Marques, *in* "Proc. Euroceramics II" (G. Ziegler and H. Hausner, Eds.), Vol. 3, p. 2179. Deutsche Keramische Gesellschaft e.V., Augsburg, 1991.
6. R. M. C. Marques, J. R. Frade, and F. M. B. Marques, *Bol. Soc. Esp. Ceram. Vid.* **30,** 464 (1991).
7. H. Naito and H. Arashi, *Solid State Ionics* **53–56,** 436 (1992).
8. M. T. Colomer, J. R. Jurado, R. M. C. Marques, F. M. B. Marques, *in* "Proc. Third Int. Symp. on Solid Oxide Fuel Cells," (S. C. Singhal and H. Iwahara, Eds.), Vol. 93–94, p. 523. Electrochem. Soc. Inc., Pennington, NJ, 1993.
9. T. Lindegaard, C. Clausen, and M. Mogensen, *in* "14th Riso International Symp. on Materials Science," (F. W. Poulsen, J. J. Bentzen, T. Jacobsen, E. Skou, and M. J. L. Ostergard, Eds.), p. 311. Riso National Laboratory, Roskilde, 1993.
10. K. Swider and W. L. Worrell, *J. Electrochem. Soc.* **143,** 3706 (1996).
11. M. Hrovat, J. Holc, and D. Kolar, *Solid State Ionics* **68,** 99 (1993).
12. M. T. Colomer and J. R. Jurado, *J. Solid State Chem.* **141,** 282 (1998).
13. P. Han and W. L. Worrell, *J. Electrochem. Soc.* **143,** 3706 (1996).
14. H. Iwahara, T. Esaka, and K. Takeda, *in* "Advances in Ceramics: Science and Technology of Zirconia III," Vol. 24, pp. 907–914. Amer. Ceram. Soc. Columbus, OH, 1988.
15. N. Matsui and M. Takigawa, *Solid State Ionics* **40–41,** 926 (1990).
16. J. H. Kim and G. M. Choi, *Solid State Ionics* **130,** 157 (2000).
17. M. T. Colomer, P. Durán, A. Caballero, and J. R. Jurado, *Mater. Sci. Eng. A* **229,** 114 (1997).
18. L. S. M. Traqueia, T. Pagnier, and F. M. B. Marques, *J. Europ. Ceram. Soc.* **17,** 1019 (1997).
19. R. M. C. Marques, F. M. B. Marques, and J. R. Frade, *Solid State Ionics* **73,** 27 (1994).
20. R. A. Miller, J. L. Smialek, and R. G. Garlick, *in* "Advances in Ceramics," (A. H. Heuer and L. W. Hobbs, Eds.), Vol. 3, pp. 291–253. Amer. Ceram. Soc., Columbus, OH, 1981.
21. F. M. B. Marques and G. P. Wirtz, *J. Am. Ceram. Soc.* **75,** 369 (1992).
22. P. Li, I. W. Chei, and J. E. Penner-Hahn, *J. Am. Ceram. Soc.* **77,** 1281 (1994).
23. K. C. Radford and R. J. Bratton, *J. Mater. Sci.* **14,** 59 (1979).
24. R. D. Shannon, *Acta Cryst allogr. Sect. A* **32,** 751 (1976).
25. A. J. Feighery, J. T. S. Irvine, D. P. Fagg, and A. Kaiser, *J. Solid State Chem.* **143,** 273 (1999).
26. M. T. Colomer, Ph.D. thesis. Autonoma University, Madrid, 1995.
27. M. T. Colomer, J. R. Jurado, R. M. C. Marques, and F. M. B. Marques, *in* Proceedings of the 2nd Intern. Symp. On Ionic and Mixed Conducting Ceramics, edited by T.A. Ramanarayanan, W.L. Worrell, and H.L. Tuller., (The Electrochem. Soc. Inc., Vol. 94 Pennington, NJ, 1994), p. 369.
28. M. T. Colomer, L. S. M. Traqueia, J. R. Jurado, and F. M. B. Marques, *Mater. Res. Bull.* **30,** 515 (1995).
29. R. M. C. Marques, F. M. B. Marques, and J. R. Frade, *in* "Proc. 3rd. Int. Symp. On SOFC" (S. C. Singhal and H. Iwahara, Eds.), Vol. 93–94, p. 513. Electrochem. Soc. Inc., Pennington, NJ, 1993.
30. J. W. Patterson, E. C. Bogren, and R. A. Rapp, *J. Electrochem. Soc.* **114,** 752 (1967).
31. I. G. Austin and N. F. Mott, *Adv. Phys.* **18,** 41 (1969).